IEEE Access
Multidisciplinary | Rapid Review | Open Access Journal

Received December 30, 2021, accepted January 13, 2022, date of publication January 18, 2022, date of current version January 27, 2022.

Digital Object Identifier 10.1109/ACCESS.2022.3144404

Static Deflection Compensation of Multi-Link Flexible Manipulators Under Gravity

DIPENDRA SUBEDI, TEODOR NILSEN AUNE, ILYA TYAPIN, AND GEIR HOVLAND
Department of Engineering Sciences, University of Agder, 4879 Grimstad, Norway
Corresponding author: Dipendra Subedi (dipendra.subedi@uia.no)

This work was partially funded by the Research Council of Norway through the centre SFI Offshore Mechatronics, project 237896.

ABSTRACT The static deflection compensation method of a planar multi-link flexible manipulator is proposed using the feedback from inertial sensors mounted at the tip of each link. The proposed compensation technique is validated experimentally using a high-precision laser tracker. The proposed strategy is experimentally verified using a three-link flexible manipulator. A strategy to compensate for the centripetal and tangential acceleration induced on the accelerometer mounted on the rotating link is proposed for correct inclination estimation. The improvement in the inclination estimation using the proposed compensation technique is verified both in simulation and experimental studies.

INDEX TERMS Flexible arm, elasticity, oscillations, deflection compensation, 3DoF manipulator.

I. INTRODUCTION

The interest in using long-reach manipulators for different applications has increased significantly in recent years [1]. Because of the use of elastic material and slender design of the arm, link flexibility is introduced in the manipulator system. This causes static (due to gravity) and dynamic (oscillations) deflections of the end-effector.

The end-effector control of the flexible link manipulator (FLM) is more difficult than the rigid link manipulator because of the presence of unwanted deflections and vibrations in the FLM. The rigid body kinematics and joint position feedback are not enough for the precise position and orientation control of the FLMs. Additional sensors (e.g. inertial sensors and vision sensors) are therefore required to be integrated into the FLM control architecture to sense deflections and oscillations. For correct end-effector positioning in the FLM, the deflection should be estimated by using a suitable sensor system and should be compensated using a feedback control strategy of adjusting joint variables.

There are many methods to estimate flexible deformation, including strain gauges, inertial measurement units (IMUs), optical/vision systems, position sensitive devices, piezoelectric materials, ultrasonic sensors, and range sensors [2]. Each of these sensor systems has associated merits and limitations. A vision system that can capture the deformed shape of the flexible link may take a long processing time which makes it unsuitable for real-time applications [3]. Additionally, the optical sensor systems are obstructed when an object comes in between the camera and the FLM [4]. The strain gauges are versatile and accurate but are difficult to install properly as they must be perfectly bonded to the material across the entire face to strain with the link. Moreover, the electronics necessary to amplify the signal and acquire the data are costly. Strain gauges are susceptible to temperature drift and have a drawback of excess wiring when many of them are used. The IMU (accelerometer and gyroscope) allows the system to know the true course of motion and can be used to obtain the position, velocity, and acceleration estimations (considering the joint encoder readings are available).

The static deformation-compensation method based on inclination-sensor feedback is presented in [5]. The accelerometers are used for the estimation of flexural states of a macro-micro manipulator in [3]. Although the inertial sensors, placed typically at the tip of the flexible link, are used for measuring oscillations; they have not been used for measuring static deflections [4]. Several optical sensing systems have been used for measuring the link deflections [6]–[10]. The strain gauges that are strategically placed along a link are the sensor systems used to estimate the deflections indirectly [4], [11], [12].

The use of an IMU mounted at the tip of each flexible link is highlighted in this paper for measuring the deflection of the flexible link. The static deflection compensation using the tip-mounted inertial sensor is validated using a high-precision laser tracker. The proposed strategy

The associate editor coordinating the review of this manuscript and approving it for publication was Agustin Leobardo Herrera-May.

TABLE 1. DH parameters.

Axis	TranZ	RotZ	TranX	RotX
1	0.0	q_1	ℓ_1	0.0
2	0.0	q_2	ℓ_2	0.0
3	0.0	q_3	ℓ_3	0.0

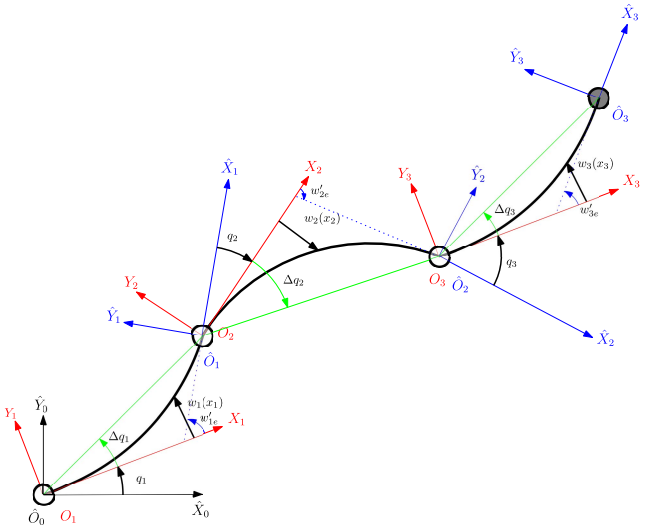

FIGURE 1. Planar three-link flexible manipulator.

is experimentally verified in a planar three-link flexible manipulator.

Inclination estimation using an accelerometer uses the gravity vector and its projection on the axes of the accelerometer to determine the tilt angle [13]. Rotating an accelerometer through gravity changes the projection of gravity on the axes of interest due to centripetal acceleration induced on the accelerometer. This results in the incorrect calculation of the inclination. A strategy is proposed in this paper to compensate for the centripetal and tangential acceleration induced on the accelerometer mounted on the rotating link for correct inclination estimation. Furthermore, the improvement in the inclination estimation using the proposed compensation technique is verified both in simulation and experimental studies.

The paper is organized into five sections as follows. The kinematic model of the three-link flexible manipulator is described in section II. The independent joint control of FLM with static deflection compensation using link-mounted IMU is elaborated in section III. The results obtained from the simulation and experimental studies are presented in section IV. Conclusions and discussions follow in section V.

II. KINEMATIC MODELING

Fig. 1 shows a planar three-link flexible manipulator with coordinate frames assigned as in [14] and Fig. 2 shows its rigid body schematic with Denavit-Hartenberg (DH) parameters given in Table 1. The kinematic model of the planar multi-link flexible manipulator is presented in [14].

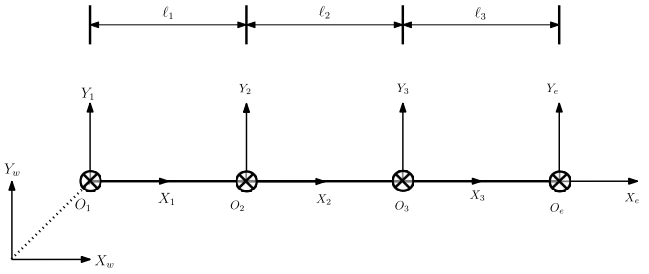

FIGURE 2. Equivalent rigid body kinematics.

The rigid motion of link i is represented by the joint i position q_i, and the deflection at any point x_i along the link i is described by $w_i(x_i)$, where $0 \leq x_i \leq \ell_i$, and ℓ_i is the length of the link i. The slope of the deflection curve at any point x_i along the link i and at its endpoint is given by (1) and (2) respectively. The angular deflection estimated (by an inertial sensor) at the tip of link i corresponds to $arctan(w'_{ie}) \approx w'_{ie}$ considering small link deflection. Moreover, when ℓ_i is not large and deformation is small then $w'_{ie} \approx \Delta q_i$, where Δq_i is the static compensation angle [5].

$$w'_i = \frac{\partial w_i(x_i)}{\partial x_i} \tag{1}$$

$$w'_{ie} = \left.\frac{\partial w_i(x_i)}{\partial x_i}\right|_{x_i=\ell_i} \tag{2}$$

From Fig. 1, it is visible that there is some error introduced when using $w'_{ie} \approx \Delta q_i$ for static deflection compensation, as $w'_{ie} > \Delta q_i$ in reality. It results in the overcompensation of the static deflection. However, this method is a good trade-off between accuracy and cost. Moreover, it is a good compromise between the complexity (and cost) of determining accurate deflection and the simplicity of neglecting the static deflection.

III. CONTROL

A. TRAJECTORY GENERATION

Apart from knowing the initial and final joint configuration of the robot, it is desirable for the motion of each joint to be smooth from the initial to the final configuration. Jerky and rough motions cause unwanted vibrations and may excite resonances in the manipulator. There are many methods of generating smooth joint trajectories as discussed in [15]. One of the methods is by defining the function that is continuous and has continuous first and higher-order derivatives. In this paper, a quintic polynomial $q_{i_d}(t)$ is used to generate the desired trajectory of joint i from the initial joint position q_{i_0} to final joint position q_{i_f} as given in (3). Here, $\dot{q}_{i_0}$, $\dot{q}_{i_f}$, $\ddot{q}_{i_0}$, and $\ddot{q}_{i_f}$ are the initial ($t = t_0 = 0$) and final ($t = t_f$) joint velocities and accelerations. For generating a trajectory for rest to rest motion, zero velocity and acceleration boundary conditions are used, i.e., $\dot{q}_{i_0} = \dot{q}_{i_f} = \ddot{q}_{i_0} = \ddot{q}_{i_f} = 0$.

$$q_{i_d}(t) = a_0 + a_1 t + a_2 t^2 + a_3 t^3 + a_4 t^4 + a_5 t^5, \tag{3}$$

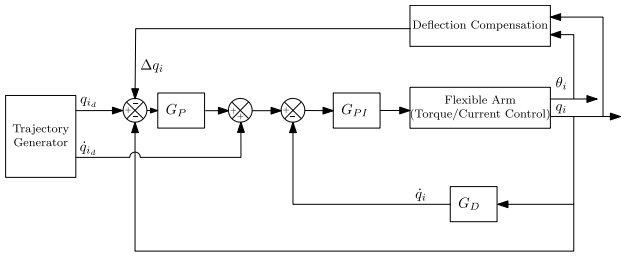

FIGURE 3. A general architecture for independent joint control with deflection compensation.

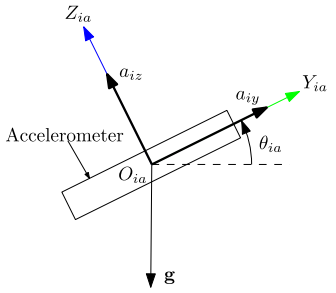

FIGURE 4. Dual-axis inclination sensing.

where,

$$a_0 = q_{i_0}, \quad a_1 = \dot{q}_0, \; a_2 = \frac{\ddot{q}_0}{2},$$

$$a_3 = \frac{20(q_{i_f} - q_{i_0}) - (8\dot{q}_{i_f} + 12\dot{q}_{i_0})t_f - (3\ddot{q}_{i_0} - \ddot{q}_{i_f})t_f^2}{2t_f^3},$$

$$a_4 = \frac{30(q_{i_0} - q_{i_f}) + (14\dot{q}_{i_f} + 16\dot{q}_{i_0})t_f + (3\ddot{q}_{i_0} - 2\ddot{q}_{i_f})t_f^2}{2t_f^4}, \text{ and}$$

$$a_5 = \frac{12(q_{i_f} - q_{i_0}) - (6\dot{q}_{i_f} + 6\dot{q}_{i_0})t_f - (\ddot{q}_{i_0} - \ddot{q}_{i_f})t_f^2}{2t_f^5}.$$

B. INDEPENDENT JOINT CONTROL

An independent joint control strategy based on a cascaded architecture is presented in [16] for rigid link manipulators and in [17] for flexible link manipulators. However, the joint position feedback used in the current paper is augmented by compensating for the slow varying static deflection caused by gravity as shown in Fig. 3. The innermost loop is a proportional-integral (PI) current controller. The next cascade level is a PI velocity control loop and the outermost cascade level is a proportional (P) position controller. The static deflection compensation action enters into the position cascade level.

The design guidelines for selecting suitable gains for the cascaded joint control topology are described in [16] and [17] for the rigid link and flexible link manipulators respectively using root locus analysis. Although the design requirements imposing large values of feedback gains may not be verified in practice because of the links' flexibilities, the smaller gain in the position feedback loop will be enough for compensating for the slow varying static deflection.

C. DEFLECTION COMPENSATION

The deflection angle must be estimated first for compensating it. The IMU mounted at the tip of each link is used for sensing the deflection.

Considering θ_i as the inclination angle estimated using IMU i, then the angular deflection $w'_{ie} \approx \Delta q_i$ of link i at the tip (or at the place where IMU is mounted on the link) is given by (4).

$$\Delta q_i = \theta_i - (q_i + \theta_{i-1}), \quad \theta_0 = 0 \tag{4}$$

The inclination angle $\theta_{ia} = arctan2(a_{iy}, a_{iz})$ estimated using the accelerometer in the range $(-\pi, \pi]$ is given by (5), where a_{iy} and a_{iz} represent accelerations measured by the accelerometer on link i along its Y-axis and Z-axis respectively. Here, the gravity vector ($\boldsymbol{g}$) and its projection on the axes of the accelerometer are used to determine the inclination angle (see Fig. 4). The accelerometers suffer from external accelerations (joint motion) that add to gravity and make the inclination estimation inaccurate. The data from the accelerometer is in general noisy and susceptible to external acceleration interference but is stable and without drift in the long term.

$$\theta_{ia} = \begin{cases} 2\arctan\left(\dfrac{a_{iy}}{\sqrt{a_{iz}^2 + a_{iy}^2} + a_{iz}}\right) & \text{if } a_{iz} > 0, \\ 2\arctan\left(\dfrac{\sqrt{a_{iz}^2 + a_{iy}^2} - a_{iz}}{a_{iy}}\right) & \text{if } a_{iz} \leq 0 \text{ and } a_{iy} \neq 0, \\ \pi & \text{if } a_{iz} < 0 \text{ and } a_{iy} = 0, \\ \text{undefined} & \text{if } a_{iz} = 0 \text{ and } a_{iy} = 0. \end{cases} \tag{5}$$

Another method to estimate the inclination angle is to integrate the output of a gyroscope. Although the gyroscope data is not susceptible to external acceleration interference like accelerometer, it drifts because of the angular velocity data bias accumulation over time. This causes an apparent rotation even when the device is stationary as the integration period is increased. So, to use the advantages of both accelerometer and gyroscope, IMU data fusion is essential for reliable and real-time inclination sensing.

The Kalman filter and the complementary filter are the most widely used IMU data fusion techniques and the latter is used in this paper. The complementary filter can be represented diagrammatically by Fig. 5 and mathematically by (6), where θ_i is the inclination angle, α_i is the filter coefficient in the range [0, 1], ω_{ig} is the angular velocity obtained from the gyroscope, T_s is the sample period, and θ_{ia} is the inclination angle obtained from the accelerometer data [18]. Here, $\alpha = \tau/(\tau + T_s)$ can be calculated using the desired time

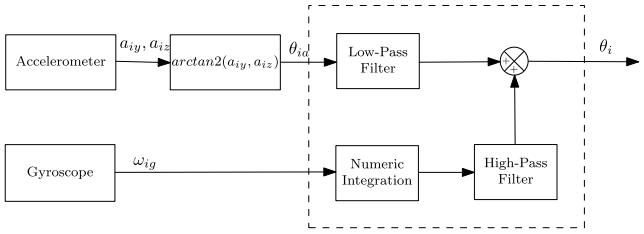

FIGURE 5. Complementary filter.

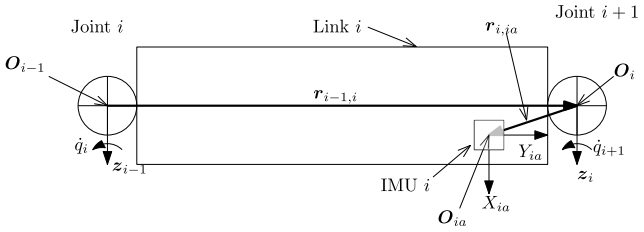

FIGURE 6. Joint i, link i, IMU i, and related definitions.

constant τ and sample period.

$$\theta_i = \alpha_i(\theta_i + \omega_{ig}T_s) + (1-\alpha_i)\theta_{ia} \tag{6}$$

1) CENTRIPETAL AND TANGENTIAL ACCELERATION

The inclination estimation from accelerometer data can be improved by removing the external acceleration (other than gravity acceleration) measured by the accelerometer. The external acceleration induced in the accelerometer mounted on the link is mainly due to the rotational joint motion. Considering the planar motion of the arm, there are two main components of the externally induced linear acceleration measured by the accelerometer mounted on the link, namely tangential acceleration (directed perpendicular to the length of the link) and centripetal acceleration (directed parallel to the length of the link).

With reference to the generic link i, shown in Fig. 6, $\boldsymbol{z}_{i-1}$ represents the unit vector along the axis of joint i, $\boldsymbol{r}_{i-1,i} = \boldsymbol{O}_i - \boldsymbol{O}_{i-1}, \boldsymbol{r}_{i,ia} = \boldsymbol{O}_{ia} - \boldsymbol{O}_i$, where $\boldsymbol{O}_i$ and $\boldsymbol{O}_{ia}$ are respectively the origin of the i-th reference frame, and reference frame of the accelerometer mounted on link i. Considering ${}^{i-1}\boldsymbol{R}_i$ be the rotation of frame i (represented by subscript) with respect to frame $i-1$ (represented by superscript), the forward recursions on the angular velocity (${}^i\boldsymbol{\omega}_i$), angular acceleration (${}^i\dot{\boldsymbol{\omega}}_i$), and linear acceleration (${}^i\dot{\boldsymbol{a}}_i$) of the frame origin of each link i are given by (7)–(9) respectively [19]. Note that the superscript represents the reference frame with respect to which the quantities (vectors and rotations) are expressed. The linear acceleration of the frame origin of the accelerometer reference frame expressed with respect to i-th reference frame and accelerometer reference frame of link i are given by (10) and (11) respectively.

$${}^i\boldsymbol{\omega}_i = {}^{i-1}\boldsymbol{R}_i^T[{}^{i-1}\boldsymbol{\omega}_{i-1} + \dot{q}_i\boldsymbol{z}_{i-1}] \tag{7}$$

$${}^i\dot{\boldsymbol{\omega}}_i = {}^{i-1}\boldsymbol{R}_i^T[{}^{i-1}\dot{\boldsymbol{\omega}}_{i-1} + \ddot{q}_i\boldsymbol{z}_{i-1} + {}^{i-1}\boldsymbol{\omega}_{i-1} \times \dot{q}_i\boldsymbol{z}_{i-1}] \tag{8}$$

$${}^i\dot{\boldsymbol{a}}_i = {}^{i-1}\boldsymbol{R}_i^T{}^{i-1}\dot{\boldsymbol{a}}_{i-1} + {}^i\dot{\boldsymbol{\omega}}_i \times {}^i\boldsymbol{r}_{i-1,i} + {}^i\boldsymbol{\omega}_i \times ({}^i\boldsymbol{\omega}_i \times {}^i\boldsymbol{r}_{i-1,i}) \tag{9}$$

$${}^i\dot{\boldsymbol{a}}_{ia} = {}^i\dot{\boldsymbol{a}}_i + {}^i\dot{\boldsymbol{\omega}}_i \times {}^i\boldsymbol{r}_{i,ia} + {}^i\boldsymbol{\omega}_i \times ({}^i\boldsymbol{\omega}_i \times {}^i\boldsymbol{r}_{i,ia}) \tag{10}$$

$${}^{ia}\dot{\boldsymbol{a}}_{ia} = {}^{ia}\boldsymbol{R}_i{}^i\dot{\boldsymbol{a}}_{ia} \tag{11}$$

where,

$$\begin{aligned} i &= 1, 2, 3 \\ \boldsymbol{z}_{i-1} &= \begin{bmatrix} 0 & 0 & 1 \end{bmatrix}^T \\ {}^i\boldsymbol{r}_{i-1,i} &= \begin{bmatrix} \ell_i & 0 & 0 \end{bmatrix}^T \\ {}^{ia}\boldsymbol{R}_i &= \begin{bmatrix} 0 & 0 & 1 \\ 1 & 0 & 0 \\ 0 & 1 & 0 \end{bmatrix} \\ {}^0\dot{\boldsymbol{a}}_0 &= \begin{bmatrix} 0 & 9.81 & 0 \end{bmatrix}^T \\ {}^0\boldsymbol{\omega}_0 &= {}^0\dot{\boldsymbol{\omega}}_0 = 0 \end{aligned}$$

Ideally, the accelerometer readings should be equal to ${}^{ia}\dot{\boldsymbol{a}}_{ia}$ assuming that the link on which it is mounted is rigid. To compensate for the centripetal and tangential acceleration induced in the accelerometer due to joint motion, we calculate ${}^{ia}\dot{\boldsymbol{a}}_{ia}$ from (7)–(11) assuming zero gravity (i.e., ${}^0\dot{\boldsymbol{a}}_0 = \begin{bmatrix} 0 & 0 & 0 \end{bmatrix}^T$) and subtract this value from the actual accelerometer readings before using them for computing the inclination. In this way, the inclination estimations from the accelerometer measurement and inclination obtained from the complementary filter after compensating for the joint-induced accelerations are more accurate compared to the estimations done without the compensation.

IV. EXPERIMENTAL SETUP AND RESULTS

The experimental setup used in this study is shown in Fig. 7. It consists of a planar three-link flexible manipulator with three revolute joints. Each link of the flexible arm is made of a hollow aluminium profile of length $\ell_1 = \ell_2 = \ell_3 = 1.5$ m. Each joint consists of a hub, motor, and planetary gearbox. The STIM300 IMU sensor is mounted closer to the tip of each link (${}^1\boldsymbol{r}_{1,1a} = \begin{bmatrix} -0.185 & 0.035 & 0.0198 \end{bmatrix}^T$ m, ${}^2\boldsymbol{r}_{2,2a} = \begin{bmatrix} -0.160 & 0.030 & 0.0198 \end{bmatrix}^T$ m, ${}^3\boldsymbol{r}_{3,3a} = \begin{bmatrix} -0.063 & 0.025 & 0.0198 \end{bmatrix}^T$ m) and the Leica spherical reflector is mounted closer to the tip of the last link (${}^3\boldsymbol{r}_{3,3L} = \begin{bmatrix} -0.175 & 0.0430 & 0 \end{bmatrix}^T$ m) so that Leica AT960 laser tracker can track the precise position of the reflector. The Leica tracker is used for validating the deflection compensation method proposed in this paper. The Leica tracker is calibrated with respect to the inertial frame $(\widehat{X}_0, \widehat{Y}_0)$ so that the reflector position with respect to the inertial frame could be measured using the tracker.

To validate the inclination estimation using the accelerometer mounted on each link, all three links are considered rigid. The joint position, velocity, and acceleration trajectories used in the simulation are shown in Figs. 8, 9, 10 respectively. The joint trajectories are obtained using (3), where the joints are moved from rest to rest ($\dot{\boldsymbol{q}}_0 = \dot{\boldsymbol{q}}_f = \begin{bmatrix} 0 & 0 & 0 \end{bmatrix}^T$ deg/s, $\ddot{\boldsymbol{q}}_0 = \ddot{\boldsymbol{q}}_f = \begin{bmatrix} 0 & 0 & 0 \end{bmatrix}^T$ deg/s^2) from initial joint positions

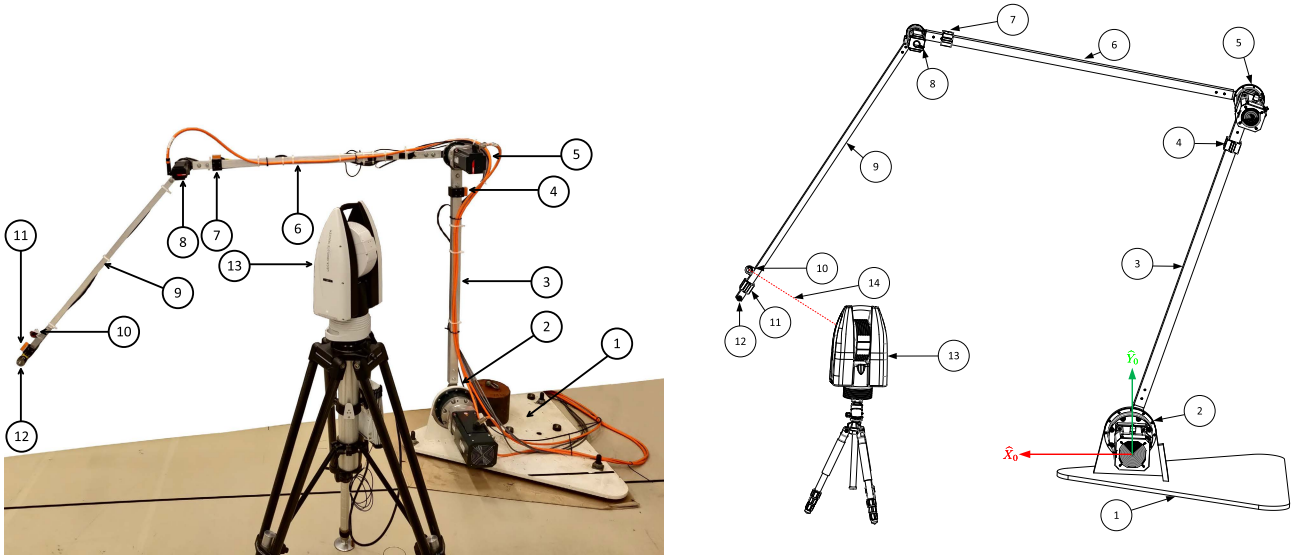

(a) (b)

FIGURE 7. Experimental setup (1. Robot base, 2. Joint 1, 3. Link 1, 4. IMU 1, 5. Joint 2, 6. Link 2, 7. IMU 2, 8. Joint 3, 9. Link 3, 10. Leica spherical reflector, 11. IMU 3, 12. Payload, 13. Leica AT960 laser tracker, 14. Laser beam): (a) actual, (b) the schematic.

$\boldsymbol{q}_0 = \begin{bmatrix}90 & -90 & -45\end{bmatrix}^T$ deg to final joint positions $\boldsymbol{q}_f = \begin{bmatrix}80 & -45 & -90\end{bmatrix}^T$ deg in $t_f = 1$ s.

The linear acceleration of the origin of the accelerometer reference frame with respect to the same frame is calculated using (7)–(11), which is shown in Figs. 11–13. Then the inclination angle of each link is calculated using (5).

For compensating for the acceleration induced due to joint motion, the linear acceleration of the origin of the accelerometer reference frame with respect to the same frame is calculated again using (7)–(11) by assuming zero gravity to obtain the acceleration caused due to joint motion alone, which is shown in Figs. 14–16. Thus obtained acceleration is subtracted from the total acceleration (along with gravity) to compensate for the acceleration induced due to joint motion. This compensated acceleration is used to obtain the inclination angle more accurately compared to the inclination calculated without compensation.

The inclination estimation using the proposed centripetal and tangential acceleration compensation method, as shown in Fig. 18, is validated with the inclination estimated using the joint position values as shown in Fig. 19. The inclination angle calculated without compensation as shown in Fig. 17 is inaccurate (see Fig. 19 as reference inclination for comparison) due to external acceleration interference (caused by joint motion).

In the experimental studies of static deflection compensation, the joints are moved from rest to rest ($\dot{\boldsymbol{q}}_0 = \dot{\boldsymbol{q}}_f = \begin{bmatrix}0 & 0 & 0\end{bmatrix}^T$ deg/s, $\ddot{\boldsymbol{q}}_0 = \ddot{\boldsymbol{q}}_f = \begin{bmatrix}0 & 0 & 0\end{bmatrix}^T$ deg/s^2) from initial joint positions $\boldsymbol{q}_0 = \begin{bmatrix}90 & -90 & -45\end{bmatrix}^T$ deg to final joint positions $\boldsymbol{q}_f = \begin{bmatrix}80 & -45 & -90\end{bmatrix}^T$ deg in $t_f = 5$ s, as shown in Fig. 20.

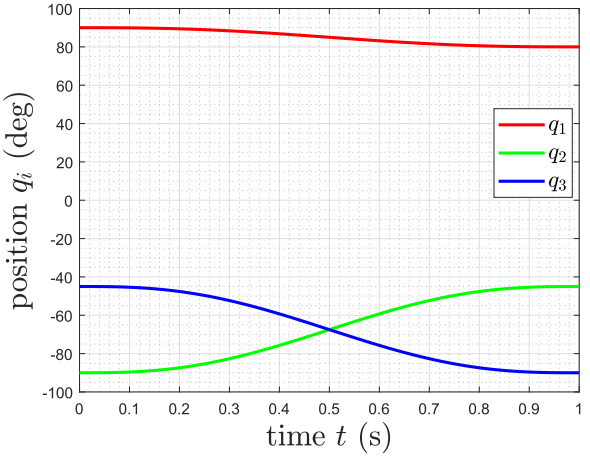

FIGURE 8. Joint position trajectory used for evaluating the performance of inclination angle estimation with joint-induced acceleration compensation in simulation.

The static deflection estimated after joint-induced acceleration compensation is shown in Fig. 21. A first-order low pass filter is used with a cut-off frequency at 0.1 Hz in the estimated static deflection to obtain a smooth signal that is then used for compensation. To validate the effect of static deflection compensation, the reflector position is measured using the Leica AT960 laser tracker. The reflector positions measured using Leica tracker with respect to the robot reference frame ($\widehat{X}_0, \widehat{Y}_0$) with and without static deflection compensation are shown in Figs. 22 and 23. Moreover, the reference reflector position calculated using forward kinematics with reference joint position is also shown to verify the effectiveness of the static compensation. Figs. 24

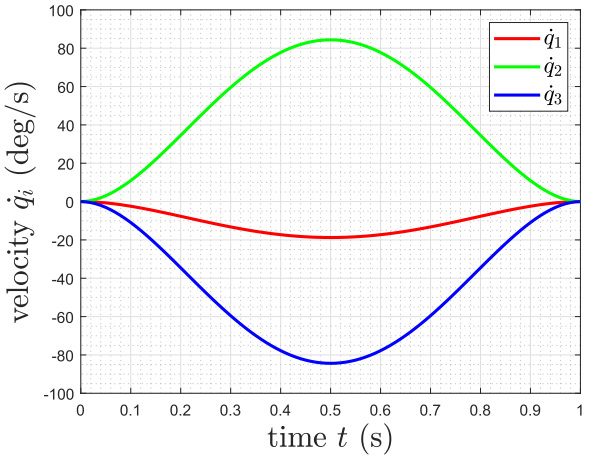

FIGURE 9. Joint velocity trajectory used for evaluating the performance of inclination angle estimation with joint-induced acceleration compensation in simulation.

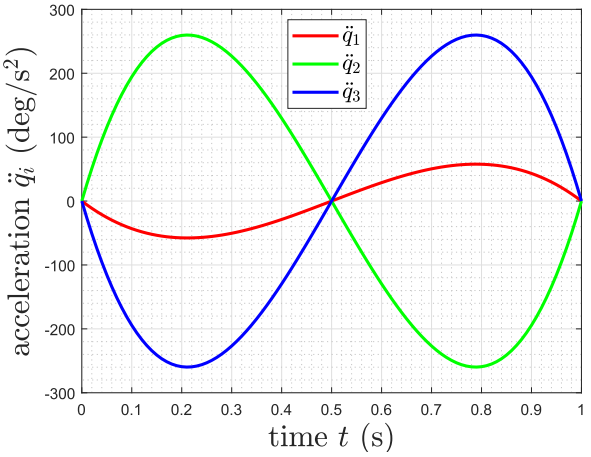

FIGURE 10. Joint acceleration trajectory used for evaluating the performance of inclination angle estimation with joint-induced acceleration compensation in simulation.

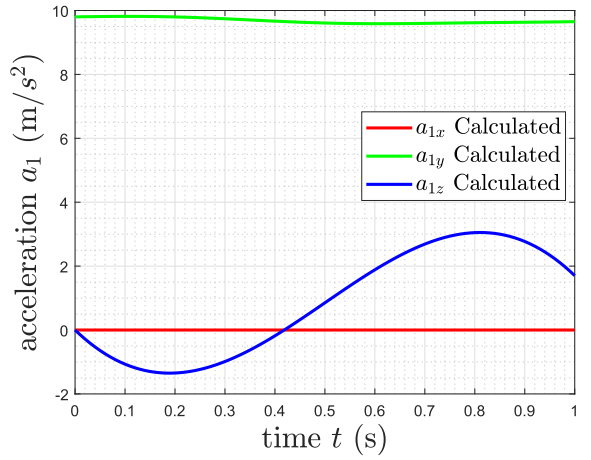

FIGURE 11. Link 1 accelerometer readings calculated with gravity in simulation.

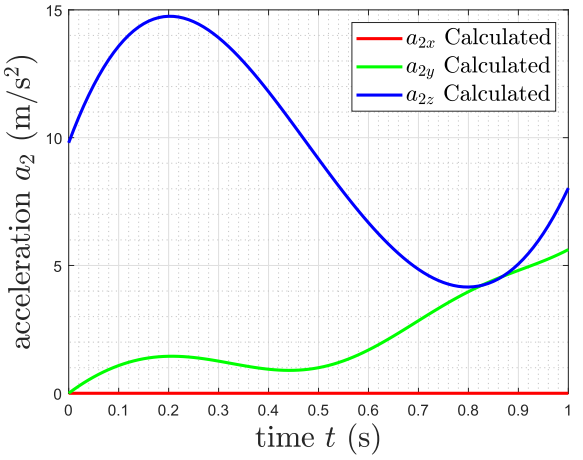

FIGURE 12. Link 2 accelerometer readings calculated with gravity in simulation.

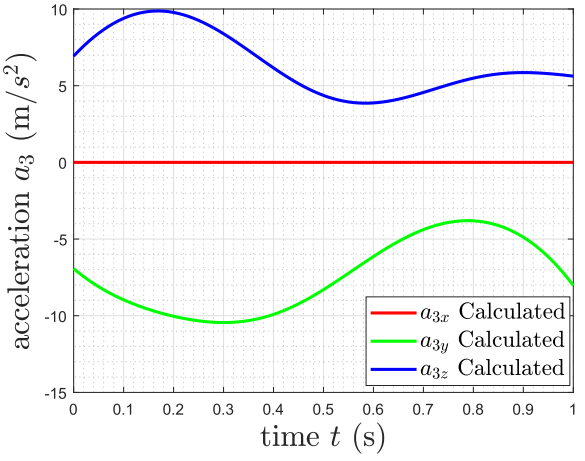

FIGURE 13. Link 3 accelerometer readings calculated with gravity in simulation.

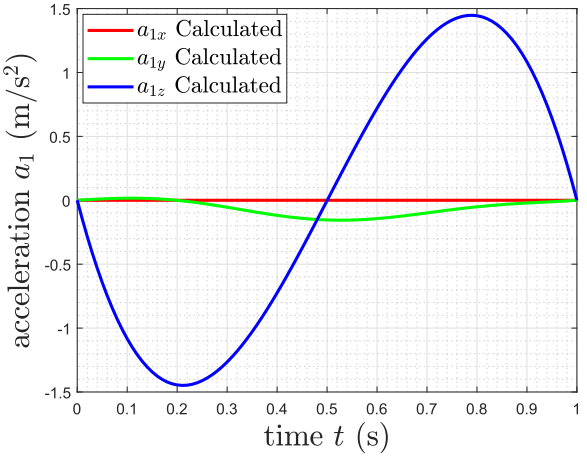

FIGURE 14. Link 1 accelerometer readings calculated assuming zero gravity in simulation.

and 25 show the error in x and y position of the reflector with and without static deflection compensation obtained by calculating the difference between the reference position and the actual position of the reflector. The error in Fig. 25 is the result of overcompensation of the static deflection by using $w'_{ie} \approx \Delta q_i$ for static deflection compensation, as $w'_{ie} > \Delta q_i$

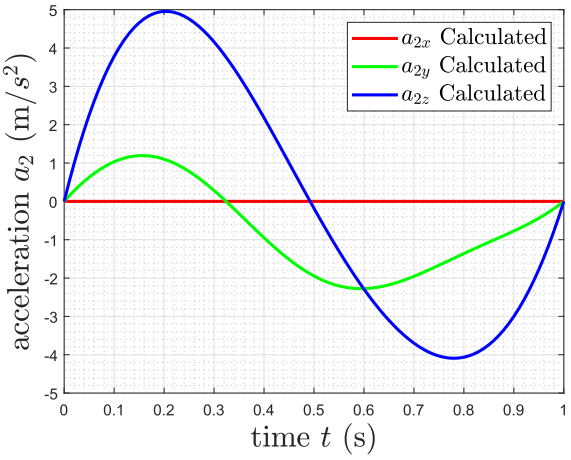

FIGURE 15. Link 2 accelerometer readings calculated assuming zero gravity in simulation.

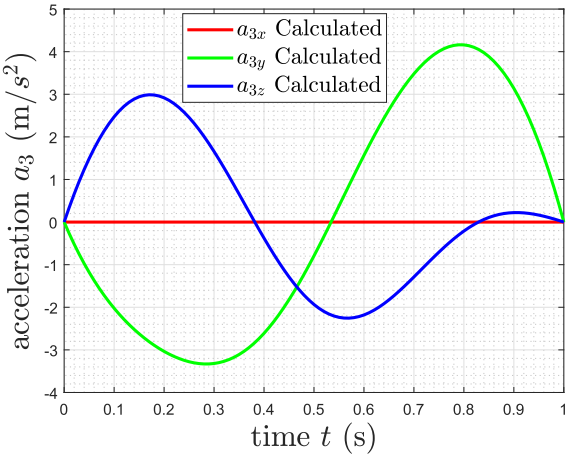

FIGURE 16. Link 3 accelerometer readings calculated assuming zero gravity in simulation.

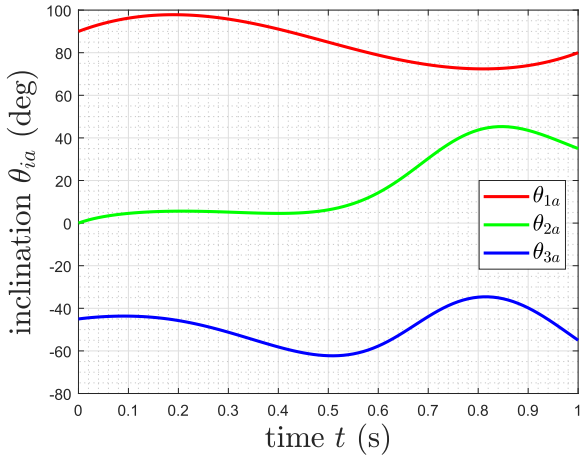

FIGURE 17. Uncompensated inclination angle from the accelerometer in simulation.

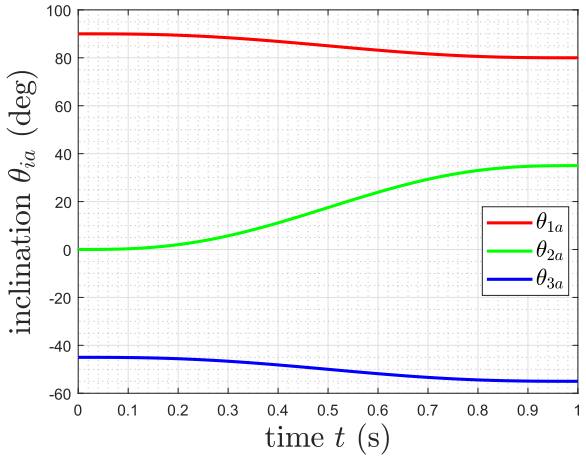

FIGURE 18. Compensated inclination angle from the accelerometer in simulation.

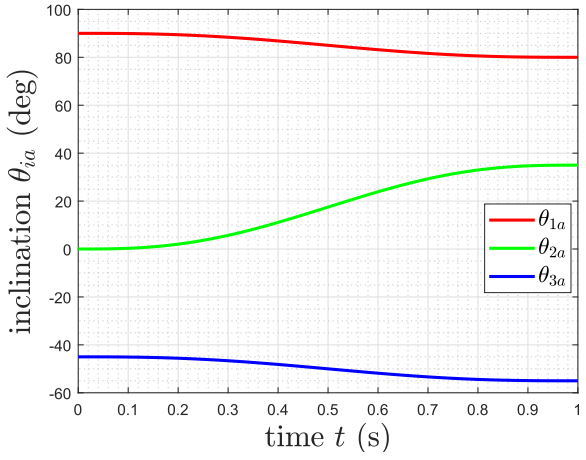

FIGURE 19. Inclination angle calculated using joint position in simulation.

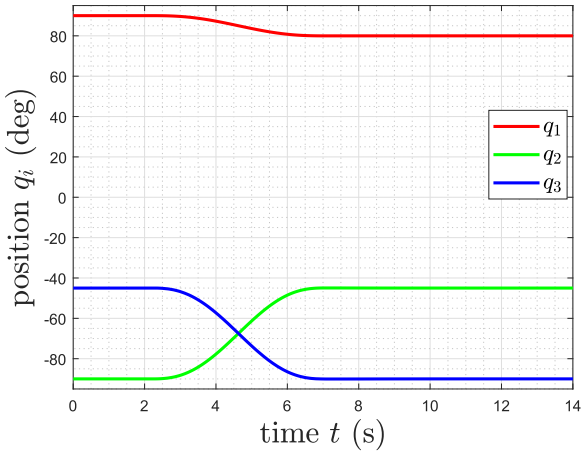

FIGURE 20. Joint position trajectory used for evaluating the performance of static deflection compensation.

in reality (see Fig. 1). Since the error in Fig. 25 is marginal, the proposed method is proved to be a good compromise between the complexity (and cost) of determining accurate deflection and the simplicity of neglecting the static deflection.

The joint-induced acceleration compensation in the link mounted accelerometer readings is verified experimentally by moving joints 3 from −90 deg to 0 deg in 2 s and keeping the other two joints stationary as shown in Fig. 26. Fig. 27

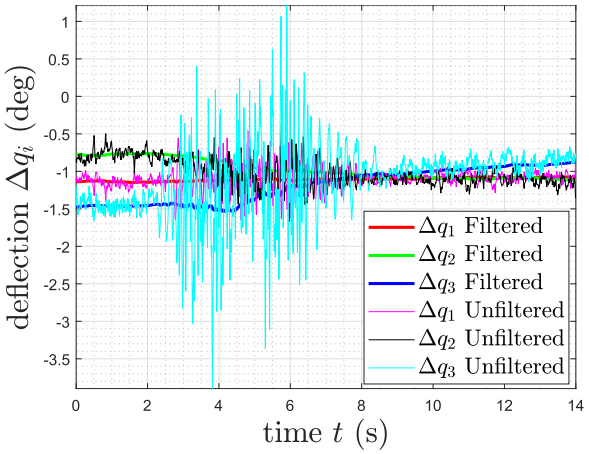

FIGURE 21. Link deflections.

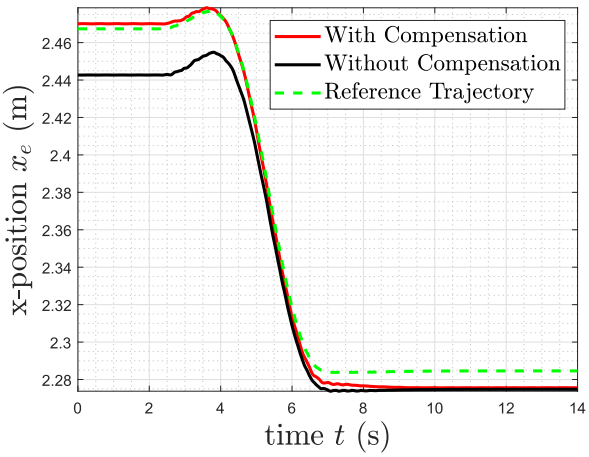

FIGURE 22. Reflector x-position measured using laser tracker with and without static deflection compensation.

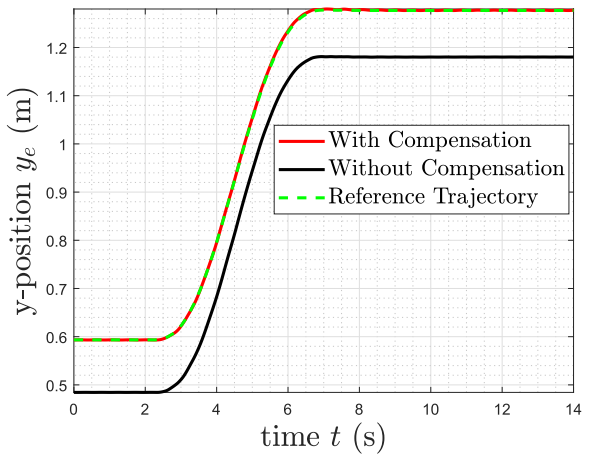

FIGURE 23. Reflector y-position measured using laser tracker with and without static deflection compensation.

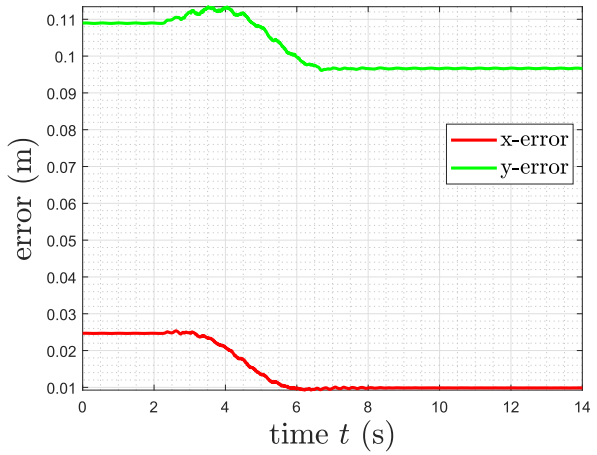

FIGURE 24. Reflector position error without static deflection compensation.

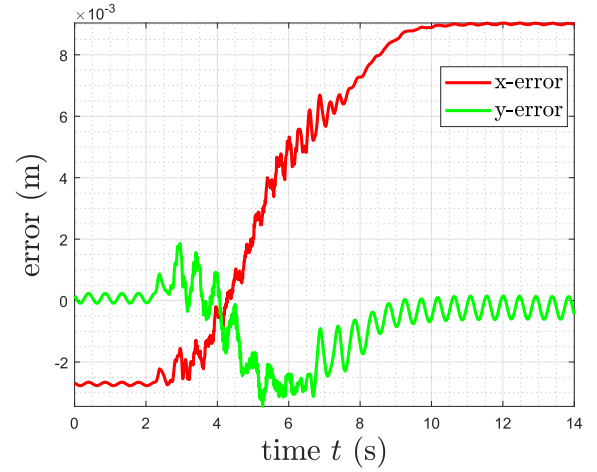

FIGURE 25. Reflector position error with static deflection compensation.

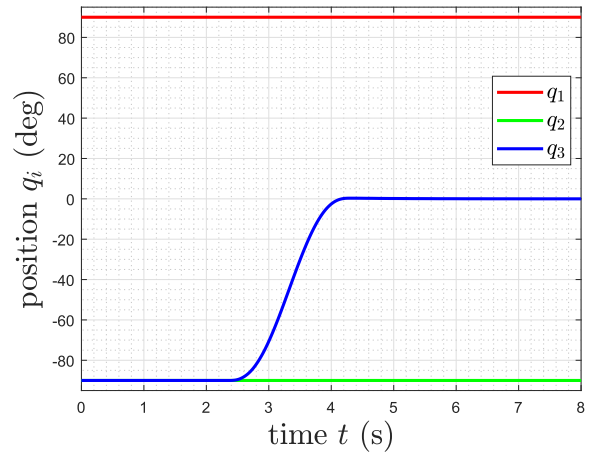

FIGURE 26. Joint position trajectory used for evaluating the performance of deflection estimation with joint-induced acceleration compensation.

shows the linear acceleration measured by the accelerometer mounted on link 3 and the acceleration computed using (7)–(11). The measured and calculated acceleration values at the origin of the accelerometer, shown in Fig. 27, are almost overlapping apart from the error introduced due to the rigid link assumption while calculating the acceleration.

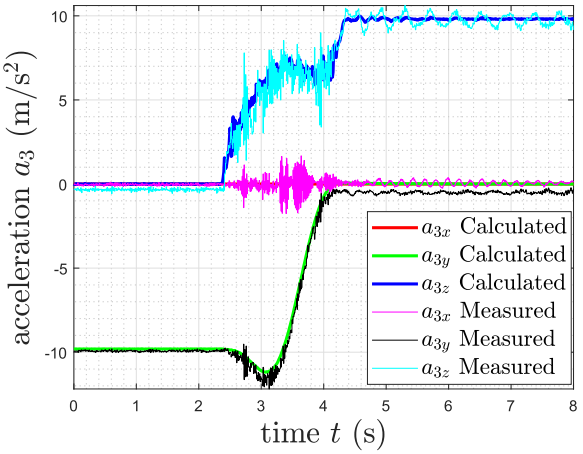

FIGURE 27. Link 3 accelerometer readings calculated vs measured.

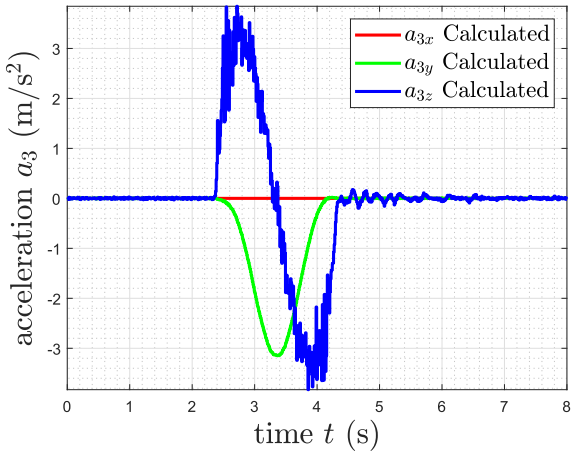

FIGURE 28. Link 3 accelerometer readings calculated assuming zero gravity.

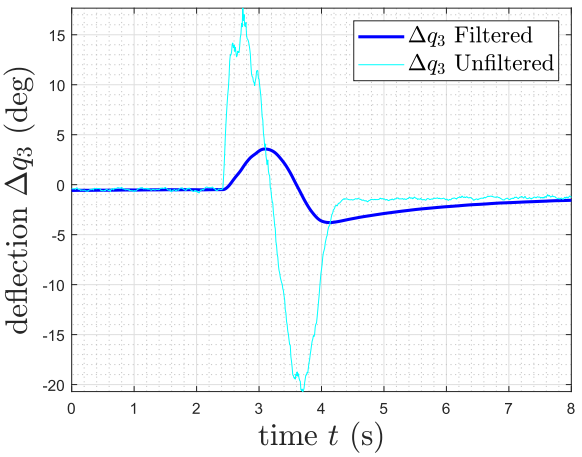

FIGURE 29. Link 3 deflection estimated without joint-induced acceleration compensation.

The linear acceleration of the origin of the accelerometer reference frame with respect to the same frame induced due to joint 3 motion only (assuming no gravity acceleration) is

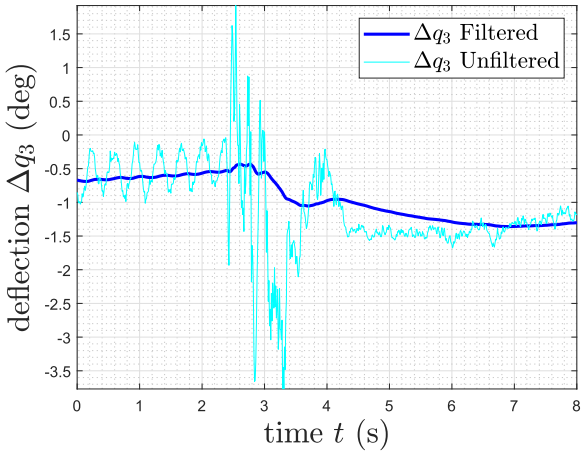

FIGURE 30. Link 3 deflection estimated with joint-induced acceleration compensation.

shown in Fig. 28. The joint-induced acceleration calculated assuming no gravity is compensated (subtracted) from the IMU readings to estimate the link deflection. Figs. 29 and 30 show the deflection of link 3 calculated without and with joint-induced acceleration compensation. A first-order low pass filter is used with a cut-off frequency at 0.1 Hz in the estimated static deflection to obtain a smooth deflection signal. The negative influence of joint motion in static deflection estimation without the joint-induced acceleration compensation is clearly visible in Fig. 29. The static deflection estimation is improved by compensating for the joint-induced acceleration as shown in Fig. 30.

V. CONCLUSION AND DISCUSSIONS

The static deflection compensation technique of planar multi-link flexible manipulators under gravity is proposed and experimentally validated. The performance of the IMU-based deflection estimation is validated using the high-precision laser tracker.

The cut-off frequency of the low pass filter used in smoothing the deflection signal should be smaller than the smallest resonance frequency of the arm while manipulating the maximum payload. This is done to avoid resonance that may occur during the compensation. It should be noted that the resonance frequencies depend on the robot configuration and the payload [14].

In the next step, the work will be extended to the implementation of oscillation damping control using the deflection signal from the IMU mounted on each link of the multi-link manipulator. Moreover, the use of the redundant degree of freedom of the planar three-link flexible arm will be explored for suppressing the elastic vibrations.

REFERENCES

[1] D. Subedi, I. Tyapin, and G. Hovland, "Review on modeling and control of flexible link manipulators," *Model., Identificat. Control, Norwegian Res. Bull.*, vol. 41, no. 3, pp. 141–163, 2020.
[2] C. T. Kiang, A. Spowage, and C. K. Yoong, "Review of control and sensor system of flexible manipulator," *J. Intell. Robot. Syst.*, vol. 77, no. 1, pp. 187–213, 2005.

[3] K. Parsa, J. Angeles, and A. K. Misra, "Estimation of the flexural states of a macro-micro manipulator using point-acceleration data," *IEEE Trans. Robot.*, vol. 21, no. 4, pp. 565–573, Aug. 2005.
[4] I. Payo and V. Feliu, "Strain gauges based sensor system for measuring 3-D deflections of flexible beams," *Sens. Actuators A, Phys.*, vol. 217, pp. 81–94, Sep. 2014.
[5] J. Qian, Q. Su, F. Zhang, Y. Ma, Z. Fang, and B. Xu, "Static deformation-compensation method based on inclination-sensor feedback for large-scale manipulators with hydraulic actuation," *Processes*, vol. 8, no. 1, p. 81, Jan. 2020.
[6] K. Obergfell and W. J. Book, "End-point position measurements of long-reach flexible manipulators," *IFAC Proc. Volumes*, vol. 27, no. 14, pp. 669–674, Sep. 1994.
[7] W. L. Xu, S. K. Tso, and X. S. Wang, "Sensor-based deflection modeling and compensation control of flexible robotic manipulator," *Mechanism Mach. Theory*, vol. 33, no. 7, pp. 909–924, Oct. 1998.
[8] S. K. Tso, T. W. Yang, W. L. Xu, and Z. Q. Sun, "Vibration control for a flexible-link robot arm with deflection feedback," *Int. J. Non-Linear Mech.*, vol. 38, no. 1, pp. 51–62, Jan. 2003.
[9] Z.-H. Jiang and A. Goto, "Visual sensor based vibration control and end-effector control for flexible robot arms," in *Proc. IEEE Int. Conf. Ind. Technol.*, Dec. 2005, pp. 383–388.
[10] I. Weerasekera, G. Balyasin, W.-H. Zhu, and G. Liu, "Lens-less PSD measurement of flexible link deflection," *Meas. Sci. Technol.*, vol. 30, no. 1, Dec. 2018, Art. no. 015003.
[11] C. Mavroidis, P. Rowe, and S. Dubowsky, "Inferred end-point control of long reach manipulators," in *Proc. IEEE/RSJ Int. Conf. Intell. Robots Syst., Hum. Robot Interact. Cooperat. Robots*, Aug. 1995, pp. 71–76.
[12] M. H. Korayem, A. M. Shafei, and F. Absalan, "Estimate a flexible link's shape by the use of strain gauge sensors," *ISRN Robot.*, vol. 2013, pp. 1–9, Oct. 2013.
[13] C. J. Fisher, "Using an accelerometer for inclination sensing," Analog Devices, Norwood, MA, USA, Appl. Note AN-1057, 2010, pp. 1–8.
[14] D. Subedi, I. Tyapin, and G. Hovland, "Dynamic modeling of planar multi-link flexible manipulators," *Robotics*, vol. 10, no. 2, p. 70, May 2021.
[15] J. J. Craig, *Introduction to Robotics: Mechanics and Control, 3/E*. London, U.K.: Pearson, 2009.
[16] L. Sciavicco and B. Siciliano, *Modelling and Control of Robot Manipulators*. Cham, Switzerland: Springer, 2001.
[17] J. Malzahn, "Modeling and control of multi-elastic-link robots under gravity: From oscillation damping and position control to physical interaction," Ph.D. dissertation, Dept. Fac. Elect. Eng. Inf. Technol., TU Dortmund Univ., Dortmund, Germany, 2014. [Online]. Available: http://hdl.handle.net/2003/33694
[18] P. Gui, L. Tang, and S. Mukhopadhyay, "MEMS based IMU for tilting measurement: Comparison of complementary and Kalman filter based data fusion," in *Proc. IEEE 10th Conf. Ind. Electron. Appl. (ICIEA)*, Jun. 2015, pp. 2004–2009.
[19] A. D. Luca and L. Ferrajoli, "A modified Newton-euler method for dynamic computations in robot fault detection and control," in *Proc. IEEE Int. Conf. Robot. Autom.*, May 2009, pp. 3359–3364.

DIPENDRA SUBEDI received the B.E. degree in electrical and electronics engineering from Anna University, Chennai, India, in 2014, and the joint master's degree in advanced robotics from the University of Genoa, Genoa, Italy, and Jaume I University, Castellón de la Plana, Spain, in 2017. From 2017 to 2018, he worked as a Robotics Software Engineer with Dorabot Inc., where he was involved in software development for the control of manipulators. Since 2019, he has been a Ph.D. Research Fellow with the Department of Engineering Sciences, University of Agder, Norway. His research interests include flexible link manipulators, dynamics, sensor fusion, and control.

TEODOR NILSEN AUNE received the B.Sc. and M.Sc. degrees in mechatronics from the University of Agder, Grimstad, Norway, in 2015 and 2017, respectively. He is currently pursuing the industrial Ph.D. degree with the Department of Engineering Sciences, University of Agder, Norway, in collaboration with Red Rock Marine. From 2017 to 2021, he worked at Red Rock Marine as a Research and Development Engineer, where he worked with instrumentation and control system design for advanced offshore lifting equipment. His research interests include control system design, robotics, and autonomy.

ILYA TYAPIN received the Ph.D. degree in mechatronics and computer science from The University of Queensland, in 2009. From 2010 to 2011, he was a Postdoctoral Researcher with the Luleå University of Technology. From 2011 to 2014, he was also a Postdoctoral Researcher with the University of Agder, Norway, where he has been an Associate Professor in mechatronics, since 2014. His research interests include robotics, dynamics, sensor fusion, and motion control.

GEIR HOVLAND received the M.Sc. degree in engineering cybernetics from NTNU, Norway, in 1993, and the Ph.D. degree in robotics from Australian National University, in 1997. From 1997 to 2003, he was a Senior Researcher at ABB in Norway, Sweden, and Switzerland. From 2004 to 2006, he was a Senior Lecturer in mechatronics with The University of Queensland, Australia. Since 2007, he has been a Professor in mechatronics with the University of Agder, Norway. Since 2019, he has been also the CEO of the Robotics Company Hokarob AS.